https://www.scirp.org/journal/jbise
J. Biomedical Science and Engineering, 2026, Vol. 19, (No. 2), pp: 100-115

Poloxamer 188 Modulates Cytoskeletal Dynamics and Mitochondrial Reassembly during Endothelial Repair *in Vitro*

Mia Grubbs[1], Anne Alsup[1,2], Michael Cho[1]

[1]Department of Bioengineering, University of Texas at Arlington, Arlington, USA; [2]Department of Biomedical Engineering, University of Texas Southwestern, Southwestern Medical Center, Dallas, USA

Correspondence to: Michael Cho, michael.cho@uta.edu
Keywords: Poloxamer 188, Endothelial Repair, Cytoskeleton, Mitochondria, Blood Brain Barrier
Received: December 9, 2025 **Accepted:** January 31, 2026 **Published:** February 3, 2026

ABSTRACT

Poloxamer 188 (P188), a membrane sealing triblock copolymer approved by the FDA, has shown potential in tissue repair. Although mechanisms mediating P188 induced repair are increasingly better understood, its intracellular effects remain elusive. This study investigated whether P188 influences cytoskeletal remodeling and mitochondrial recovery in a brain endothelium model. Primary mouse brain microvascular endothelial cells (mBECs) were subjected to a scratch wound assay. P188 uptake was tracked with a fluorophore conjugated analog, and actin dependence was tested with pharmacological disruption. Actin remodeling was assessed by phalloidin staining, mitochondrial integrity by BioTracker 488 following injury, and cellular ATP content by luminescence assay. P188 was internalized by mBECs in an actin dependent manner, with uptake abolished by cytoskeletal disruption. Treatment enhanced lamellipodia and stress fiber formation during wound closure. P188 preserved mitochondrial mass and promoted redistribution toward the wound edge in response to injury. ATP assays confirmed improved recovery of cellular energy levels 24 h post injury compared to controls. P188 enhances endothelial wound closure not only by stabilizing membranes but also by modulating intracellular processes. By supporting cytoskeletal organization, mitochondrial redistribution, and ATP recovery, P188 facilitates coordinated structural and metabolic repair mechanisms of the brain endothelium.

1. INTRODUCTION

The blood brain barrier (BBB) is a tightly regulated vascular interface that preserves central nervous system (CNS) homeostasis by restricting the passage of potentially harmful substances while supporting

controlled nutrient exchange and signaling [1, 2]. Brain microvascular endothelial cells (BMECs), which form the cerebral endothelium, are the cellular backbone of the brain's microvasculature, where it serves as a dynamic barrier and regulatory interface between the bloodstream and neural tissue [3, 4]. Although these endothelial cells contribute to the architecture of the BBB, they also possess intrinsic reparative functions that are critical to vascular stability following injury [5, 6]. Disruption of the endothelial monolayer, whether from mechanical trauma, oxidative stress, or metabolic insult, compromises vascular continuity and leads to increased permeability, inflammatory infiltration, and tissue damage [5, 7, 8]. Prompt and efficient recovery of the endothelium is therefore essential to restoring barrier integrity and preserving local homeostasis.

To model these behaviors *in vitro*, we employed the scratch wound assay, a reproducible and widely used method for investigating collective endothelial migration and monolayer restitution [9, 10]. Disruption of the endothelial monolayer triggers directed migration of cells at the wound edge into the denuded area. These edge-localized cells, termed leader or pioneer cells, polarize in response to chemical and mechanical cues and coordinate the collective migration of follower cells [11]. Leader cells probe the extracellular environment, respond to gradients of chemoattractants, and generate protrusive force for migration. The formation of these structures is tightly regulated and depends on remodeling of both the actin and microtubule cytoskeletons [12, 13].

Directed migration is powered by dynamic remodeling of the actin cytoskeleton [14]. At the leading edge, actin polymerization drives the extension of lamellipodia and filopodia, which form new adhesions to the extracellular matrix and generate traction [15, 16]. This is accompanied by actomyosin contractility and focal adhesion disassembly at the trailing edge, allowing cells to retract and advance forward [17]. Actin polymerization is an ATP dependent process by which globular actin (G-actin) assembles into filamentous actin (F-actin), enabling rapid structural turnover and spatial control [18]. These actin based structures are orchestrated by small GTPases, Rac1, CDC42, and RhoA, and their downstream effectors including the Arp2slash3 complex, formins, and Rho associated kinase (ROCK), which coordinate filament branching, bundling, and contraction to drive migration and monolayer cohesion [19-21].

The energetic cost of cytoskeletal remodeling is high. Branching of actin filaments, focal adhesion turnover, and membrane reorganization at the leading edge all consume ATP [22]. This localized energy demand has been increasingly attributed to mitochondria, which serve as the primary source of cellular ATP, buffer intracellular calcium, and modulate reactive oxygen species (ROS) levels [23, 24]. Mitochondrial morphology and subcellular distribution are dynamically regulated by bioenergetic cues, with fission, fusion, and transport processes remodeling the mitochondrial network to meet cellular demands [25-27].

Although mitochondrial localization is considered less relevant in endothelial cells compared to highly motile cells, recent work has shown that active mitochondrial positioning is critical for cell migration [28]. Mitochondria accumulate at the leading edge where energy is most required, supplying localized ATP to support protrusion formation, adhesion dynamics, and polarity signaling [27, 29]. Schuler *et al.* (2017) demonstrated that Miro1 mediated mitochondrial trafficking to the cell periphery enhances migration by facilitating focal adhesion maturation and membrane extension [30].

The relationship between mitochondria and the cytoskeleton is bidirectional and highly coordinated, with each system influencing the structure and function of the other [31, 32]. Disruption of cytoskeletal integrity impairs mitochondrial positioning and dynamics, while mitochondrial dysfunction can hinder actin polymerization and protrusive activity [28]. This mutual dependency is especially critical during endothelial repair, when both structural remodeling and localized energy production are required for migration. Further investigation into how these systems interact during BBB endothelial wound healing is still warranted.

Poloxamer 188, a synthetic triblock copolymer consisting of a central hydrophobic chain of polyoxypropylene flanked by two hydrophilic chains of polyoxyethylene, has been widely used in pharmaceutical formulations and medical applications due to its amphiphilic structure [33]. P188 was approved by the FDA as a therapeutic reagent to reduce viscosity in the blood before transfusions [34], but since has been applied in various applications with notable potential in cellular membrane sealing with demonstrated efficacy in

models of tissue injury [35-39].

Due to its amphiphilic structure, P188 has the ability to interact with both hydrophobic and hydrophilic environments, allowing it to integrate into lipid membranes and stabilize sites of disruption [40]. While traditionally characterized as a membrane sealant acting at the plasma membrane, it has also been observed to enter cells [41]. Internalization is thought to occur through actin dependent mechanisms such as endocytosis. Once inside the cell, P188 has been shown to associate with intracellular organelles, including lysosomes and mitochondria. In these compartments, it has been reported to stabilize membrane integrity, limiting lysosomal enzyme release and preserving mitochondrial membrane potential, thereby supporting cellular recovery [42, 43]. These findings suggest that P188 may exert protective effects not only at the cell surface but also within subcellular domains essential for survival and repair.

Given the interconnected roles of the cytoskeleton and mitochondria in orchestrating endothelial migration, along with emerging evidence that P188 may influence both membrane stability and intracellular organization, we investigated its potential role in promoting endothelial repair. Using a scratch wound assay in primary mouse brain microvascular endothelial cells (mBECs), we examined whether P188 enhances wound closure by modulating cytoskeletal dynamics and supporting mitochondrial remodeling at the wound edge. This study aims to broaden our understanding of P188's intracellular effects and to evaluate its potential as a therapeutic agent for accelerating vascular recovery following injury.

Using a scratch wound assay in primary mouse brain microvascular endothelial cells, we examined whether P188 treatment enhances endothelial repair by modulating cytoskeletal dynamics and mitochondrial remodeling. Specifically, we assessed changes in actin organization at the wound edge, mitochondrial redistribution to regions of high energy demand, and overall monolayer restitution. This study aims to deepen our understanding of P188's intracellular effects and to evaluate its potential as a therapeutic agent for accelerating vascular recovery following injury.

2. MATERIALS AND METHODS

2.1. Cell Culture

BALB/c primary brain microvascular endothelial cells (mBECs) from Cell Biologics Inc (BALB-5023) were cultured in complete mouse endothelial cell medium with supplement kit (Cell Biologics Inc, M1168). Culture surfaces were precoated with gelatin coating solution (Cell Biologics Inc, 6950) according to the manufacturer's protocol. Cells were grown to 90% - 100% confluency and maintained at 37˚C in a humidified incubator with 5% CO_2.

2.2. Scratch Wound Model

Cells were seeded onto 35 mm glass bottom imaging dishes (Cellvis, D35-14-1.5-N) with a total of 50,000 cells per dish and incubated overnight. A sterile 100 µL pipette tip was used to create a linear scratch across the monolayer, and detached cells were removed by rinsing with PBS. Fresh complete medium containing 0, 10 µM, or 100 µM Poloxamer 188 (P188; Maroon Biotech, Sigma-Aldrich) was then added. Wound closure was imaged periodically using phase contrast microscopy (Nikon Eclipse Ti). For quantification, wound area at each time point was measured using FIJI ImageJ by manually tracing the cell-free region. The area was expressed as a percentage of the initial wound area at time 0, and plotted over time to calculate the rate of wound closure.

2.3. P188-Rh110 Uptake

For uptake analysis, mBECs were seeded and cultured as described above. After an overnight incubation, cells were washed with warm PBS and complete medium containing 10 µM fluorescently conjugated Poloxamer 188 (P188-Rh110) was added at the start of imaging. To disrupt actin filaments, a subset of cultures were treated with 2 µM Cytochalasin D (CyD; Sigma-Aldrich, C2618) in complete medium for 1 hour prior to P188-Rh110 addition. Live-cell fluorescence images were acquired every 1 minute for 30 minutes. Fluorescence intensity for each frame was normalized to the first frame, and mean intensity over time was

used to generate uptake curves.

2.4. Actin Cytoskeleton Imaging

To examine actin remodeling during migration, confluent mBEC monolayers were scratched as described in *2.2.* At the indicated time points, cells were fixed with Image-iT Fixative Solution (4% formaldehyde; Invitrogen, FB002) for 10 minutes, permeabilized with ice cold methanol for 10 minutes, and blocked in 1% BSA/PBS for 1 hour at room temperature. Actin architecture was visualized with Texas Red™ Phalloidin (Invitrogen, T7471), and nuclei were counterstained with NucBlue (Invitrogen, R37605). For actin disruption, cells were treated immediately post-scratch with 2 μM CyD in complete medium for 1 hour and kept at 37˚C. Then all samples were rinsed and incubated in fresh complete medium with or without 10 μM P188 for the designated post scratch treatment period before fixation. Cells were imaged using an inverted fluorescence microscope (Nikon Eclipse Ti).

2.5. Live Cell Mitochondrial Imaging

Live cell mitochondria were visualized using BioTracker 488 Green Mitochondria Dye (Sigma-Aldrich, SCT110). To induce mitochondrial depolarization, cells were treated with 5 μM Carbonyl Cyanide 3-Chlorophenylhydrazone (CCCP; Sigma-Aldrich, C2759) in complete medium for 1 hour at 37˚C, rinsed with PBS, and incubated in fresh complete medium with or without 10 μM P188. Cells were then incubated with 200 nM BioTracker dye for 30 minutes at 37˚C and imaged live. Mitochondrial fluorescence intensity was measured for individual leading-edge cells in FIJI ImageJ, and mean values were compared between treatment groups, the leading edge was defined as the first row of intact cells adjacent to the wound margin.

2.6. ATP Luminescence Assay

Cellular ATP content was measured using the ATP Determination Kit (Invitrogen, A22066) according to the manufacturer's instructions. mBECs were seeded in 96-well plates with 7500 cells per well and treated with CCCP (5 or 50 μM) for 1 hour to induce mitochondrial depolarization. After treatment, cells were rinsed and incubated in fresh complete medium with or without 10 μM P188. At the indicated time points (immediately post treatment and 24 hours later), cells were lysed with Pierce Luciferase Cell Lysis Buffer (Thermo Scientific, 16189), and luminescence was measured using a FLUOstar Omega microplate reader (BMG Labtech). Values were normalized to untreated controls, and results are expressed as fold change in luminescence intensity.

2.7. Statistical Analysis

All experiments were independently repeated three times per condition. Data were compiled in Microsoft Excel (Microsoft Corp., Redmond, WA, USA). Results are presented as mean ± SEM. Statistical significance between groups was assessed using two-tailed Student's t-tests, with $p < 0.05$ considered significant.

3. RESULTS

3.1. Validation of Monolayer Integrity Prior to Wounding

Prior to evaluating the effects of P188 on wound repair, uniform endothelial monolayer formation was confirmed, as barrier integrity and intercellular contacts are prerequisites for modeling physiologically relevant injury responses. Confluence was verified by phase contrast microscopy, with cultures consistently reaching >95% coverage by 24 h post seeding (**Figure 1(a)**). Tight junction formation was assessed by immunostaining for the junctional protein zonula occludens-1 (Zo-1). Imaging revealed continuous Zo-1 staining at cell–cell borders, indicative of intact junctional complexes across the monolayer (**Figure 1(b)**). These results confirmed that experimental wounding was performed on confluent, contact inhibited cultures, providing a consistent baseline for subsequent wound repair assays.

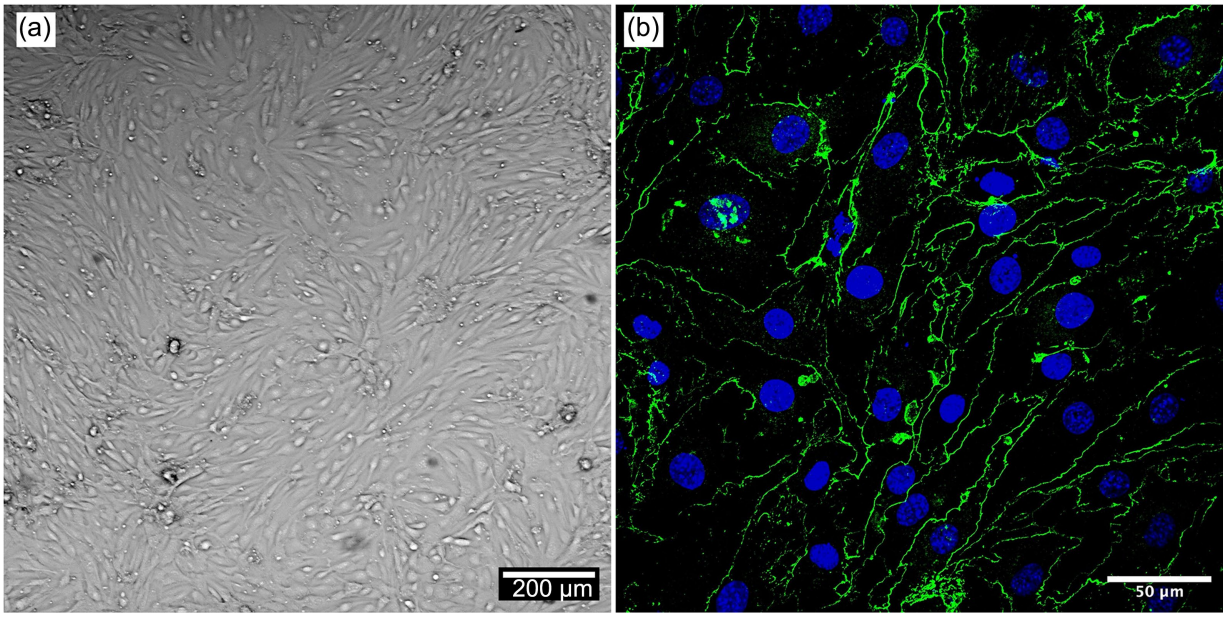

Figure 1. Representative images of mBEC monolayer confluency and tight junction formation prior to wounding. (a) Brightfield image of a confluent monolayer of mouse brain microvascular endothelial cells (mBECs) showing a uniform, contact inhibited monolayer of cells prior to scratch wounding. Scale bar = 200 µm. (b) Immunofluorescence staining of confluent mBECs using Anti-Zo-1 (green) to label the tight junction protein and DAPI (blue) to label nuclei. Zo-1 localization at cell–cell borders indicate the formation of tight junctions. Scale bar = 50 µm.

3.2. Scratch Wound Model with P188 Treatment

To evaluate whether P188 enhances endothelial repair, confluent mBEC monolayers were subjected to linear wounding and incubated with either control medium, 10 µM P188, or 100 µM P188. Wound closure was documented at 0, 6, 12, 18, and 24 h post injury using phase contrast microscopy (**Figure 2(a)**). The cell free region was traced in FIJI ImageJ, and wound area was expressed as a percentage of the initial area at time 0. Both P188 treatment groups demonstrated accelerated closure compared to controls. Quantification of wound area reduction over time revealed significantly faster closure in the presence of P188 (**Figure 2(b)**). Linear regression analysis showed closure rates of −3.50% ± 0.13%/h for media, −4.23% ± 0.20%/h for 10 µM P188, and −4.36% ± 0.29%/h for 100 µM P188 (all $R^2 > 0.97$). Differences between media and both treatment groups were statistically significant, while no difference was observed between the two P188 doses ($p > 0.7$). At individual time points, P188 treated cultures consistently showed smaller wound areas than media controls.

These findings demonstrate that P188 enhances collective migration of mBECs during wound repair. Notably, low micromolar concentrations were sufficient to elicit the maximal effect, suggesting that P188 exerts a threshold response rather than a linear dose dependent effect in this assay.

3.3. Actin Cytoskeletal Integrity Is Required for P188 Uptake

To determine whether P188 internalization depends on an intact actin cytoskeleton, uptake of fluorescently conjugated P188 (P188-Rh110) was assessed in live mBECs with or without cytochalasin D (CyD) pretreatment. Vehicle treated cells showed progressive intracellular accumulation of P188-Rh110 over 30 min, visible as punctate green fluorescence distributed throughout the cytoplasm (**Figure 3(a)**) and stress microfilament fibers (**Figure 3(b)**). In contrast, cells pretreated with 2 µM CyD showed minimal detectable copolymer signal after 30 min (**Figure 3(c)**) and exhibited fragmented actin filaments (**Figure 3(d)**).

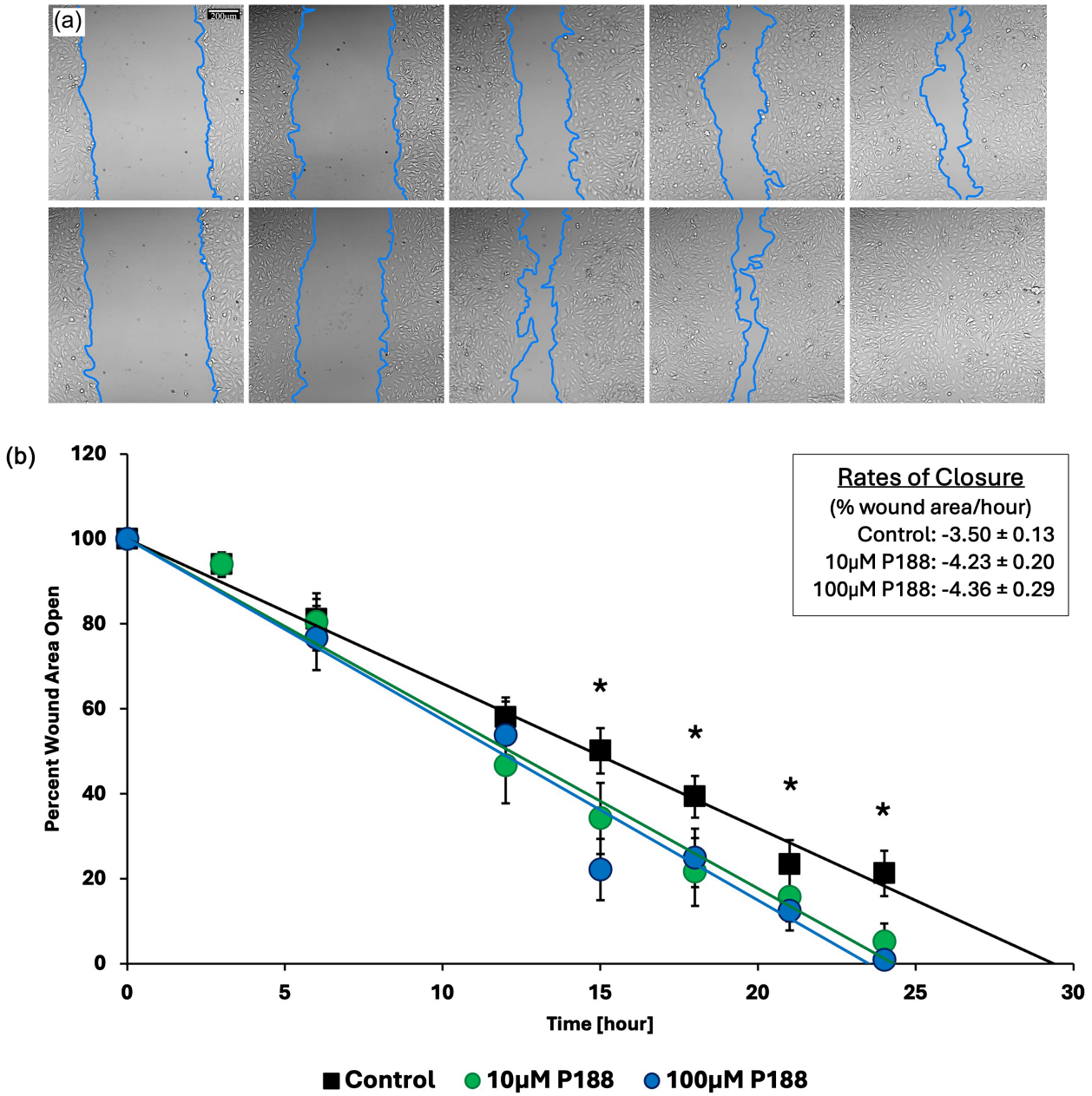

Figure 2. Poloxamer 188 accelerates wound closure in mouse brain endothelial cells (mBECs). (a) Representative phase contrast images of mBEC scratch wounds at 0, 6, 12, 18, and 24 hours post-injury in untreated control (top row) and cells treated with 10 μM P188 (bottom row). Wound margins were outlined in blue using ImageJ to quantify closure. Scale bar = 200 μm. (b) Quantification of wound closure over 24 hours in media control, 10 μM P188 (10P), and 100 μM P188 (100P) treatment groups. Data represent mean ± SEM (n = 3 per group). Linear regression analysis revealed significantly faster wound closure in both P188-treated groups compared to media. Differences in slope were significant between control and both 10P ($p < 0.05$) and 100P ($p < 0.05$), but not between 10P and 100P ($p = 0.72$), indicating an equally significant response at the lower dose of 10 μM. Asterisks (*) denote individual time points where wound area media control vs. treated were statistically significant ($p < 0.05$, two-tailed t-test).

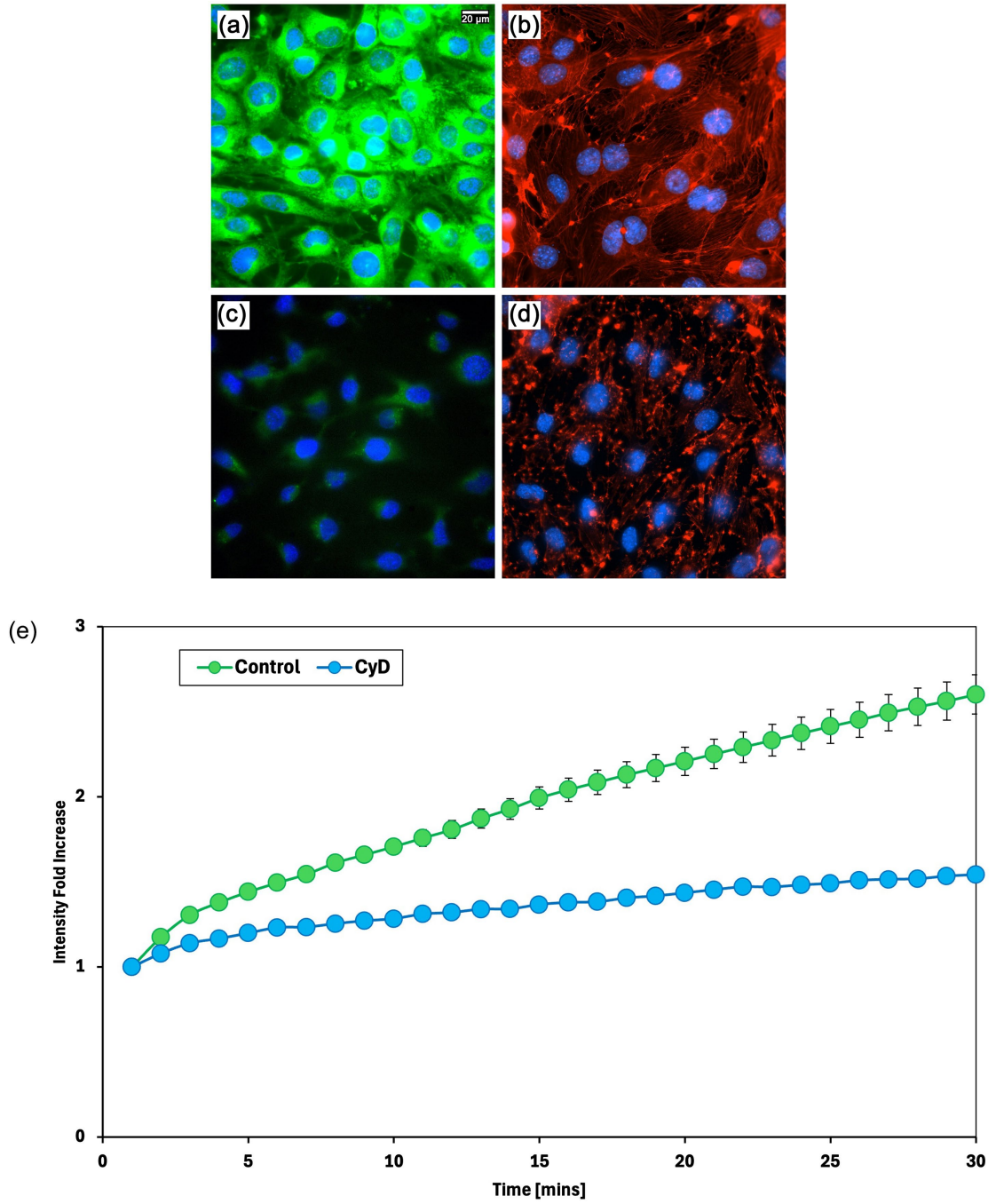

Figure 3. Actin filament integrity is required for P188-Rh110 uptake. ((a), (c)) Uptake of P188-Rh110 visualized by fluorescence microscopy, imaged and pseudo colored green to enhance contrast. Nuclei are counterstained with DAPI (blue). (a) Vehicle treated cells. (c) Cells pretreated with 2 µM Cytochalasin D for 1 hour prior to P188-Rh110 uptake. ((b), (d)) Actin cytoskeleton labeled with Texas Red-phalloidin (red) to assess filament integrity. (b) Vehicle treated cells. (d) Cells pretreated with 2 µM Cytochalasin D for 1 hour display disrupted and fragmented actin filaments, with minimal detectable polymer internalization after 30 minutes. Scale bar = 20 µm. (e) Quantification of P188-Rh110 uptake over time in mBECs treated with vehicle control (green), or Cytochalasin D (blue). Fluorescence intensity plotted as fold increased over 30 minutes. Data represent mean ± SEM, n = 3.

Quantification of uptake curves was determined by acquiring the labeled P188 images at 1 min intervals. In CyD treated cells, a marked reduction in fluorescence intensity was confirmed compared to controls (**Figure 3(e)**). In vehicle treated cells, P188-Rh110 signal increased approximately 2.5-fold over baseline after 30 min, whereas CyD treated cells showed ~20% increase and remained close to basal levels.

These findings demonstrate that P188 uptake requires intact actin filaments, suggesting that polymer internalization occurs through an active, cytoskeleton mediated process rather than passive membrane insertion. This dependence implies a functional link between actin remodeling and P188's intracellular activity during repair.

3.4. P188 Enhances Formation of Migratory Actin Structures over Time

Because actin remodeling is essential for migration, we examined whether P188 influenced cytoskeletal structures during wound repair. Confluent mBEC monolayers were scratched and stained for F-actin at 0, 6, and 24 h post injury. In media controls, actin filaments were visible but relatively sparse, with limited lamellipodia at the wound edge (**Figures 4(a)-(c)**). By contrast, cells treated with 10 μM P188 displayed progressively enhanced cytoskeletal remodeling, including broad lamellipodia and well organized stress fibers, particularly at 24 h (**Figures 4(d)-(f)**).

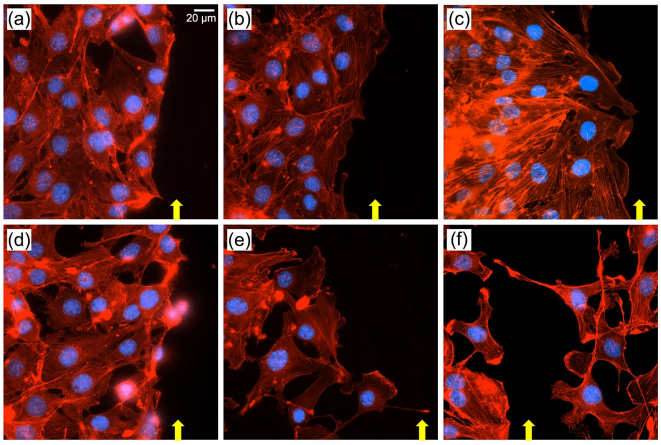

Figure 4. Actin architecture is reorganized in response to P188 treatment. Representative fluorescence images of mBECs stained with phalloidin (F-actin, red) and DAPI (nuclei, blue) at 0, 6, and 24 hours after scratch injury. Cells treated with 10 μM P188 (bottom row, (d)-(f)) exhibit progressively enhanced actin remodeling compared to media control (top row, (a)-(c)), including increased formation of lamellipodia and well defined stress fibers. By 24 hours, P188 treated cells display more pronounced protrusive structures, consistent with enhanced migratory activity. Yellow arrows indicate the wound edge in each image. Scale bar = 20 μm.

These qualitative differences in actin structures suggest that P188 supports the formation of protrusive and contractile elements at the wound margin, consistent with an enhanced migratory phenotype.

3.5. P188-Driven Cytoskeletal Remodeling and Mitochondrial Re-Organization

With emerging evidence suggesting localized energy supply is critical for migration, mitochondrial morphology and positioning were assessed in scratch wounded monolayers. In control cultures, mitochondria were primarily clustered in perinuclear regions with limited extension toward the wound edge (**Figure 5(a)** and **Figure 5(b)**). CCCP treatment induced fragmentation, resulting in a punctate, disorganized distribution (**Figure 5(c)**). In contrast, cells treated with 10 μM P188 displayed elongated, branched mitochondrial structures that extended toward the wound margin (**Figure 5(d)**).

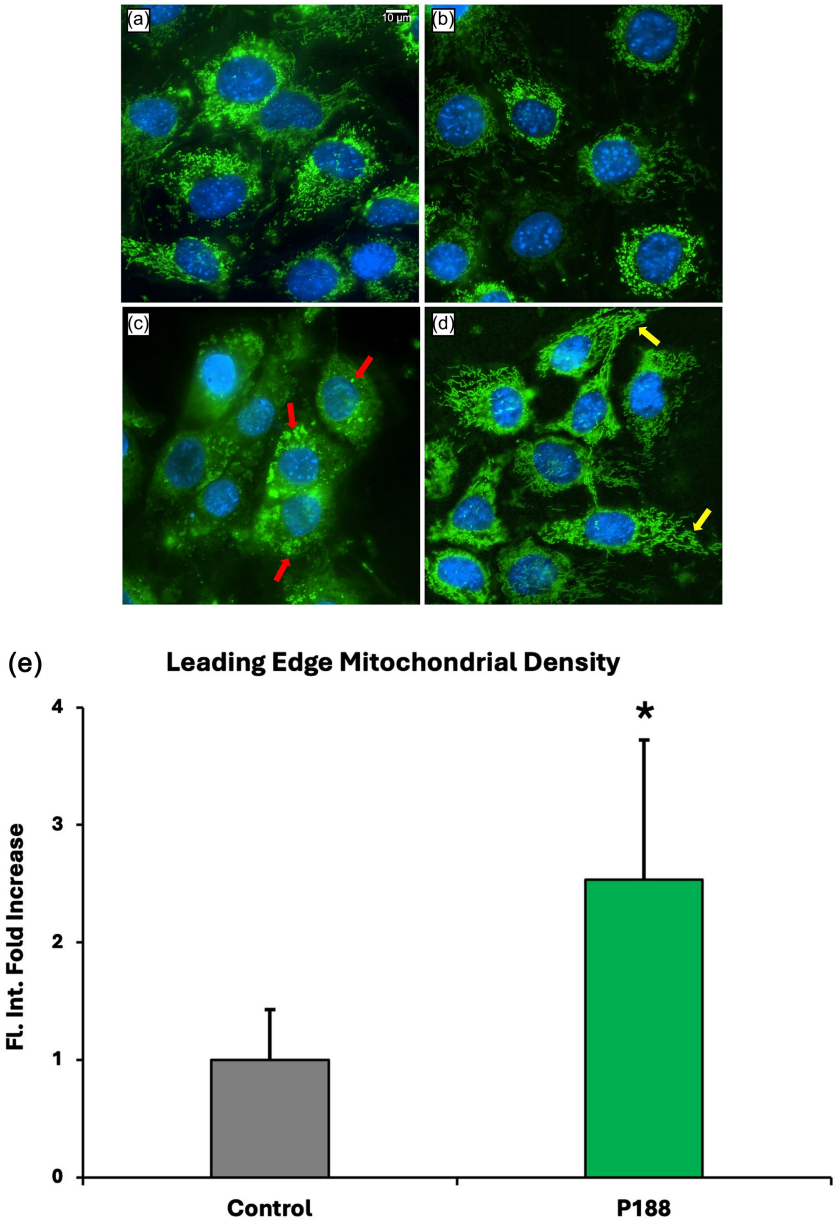

Figure 5. P188 enhances mitochondrial organization near the leading edge of migrating mBECs. ((a)-(d)) Representative fluorescence microscopy images of mBECs stained for mitochondria (green, BioTracker 488) and nuclei (blue, DAPI). (a) Undamaged control cells (top left) exhibit perinuclear mitochondrial organization with healthy structures. (c) Cells pretreated with the mitochondrial uncoupler CCCP (5 µM, 1 h; bottom left) show fragmented mitochondria (red arrows) with reduced signal intensity. Images on the right show mitochondrial localization at the leading edge of scratch wounded monolayers 24 h post injury. (b) Media treated cells display limited mitochondrial presence at the wound front, while (d) cells treated with 10 µM P188 exhibit enhanced mitochondrial density and expanded branched structure near the leading edge (yellow arrows). Scale bar = 10 µm. (e) Quantification of mitochondrial density at the wound edge 24 h post injury. P188 treated cells show a significant increase in mitochondrial fluorescence intensity compared to media controls ($p < 0.05$, unpaired t-test). Data represent mean ± SEM, n = 3.

Quantitative analysis was performed specifically on leading edge cells, defined as the first row of intact cells adjacent to the wound border. P188 treated leading edge cells exhibited significantly higher mitochondrial fluorescence intensity compared to media controls (Figure 5(e)), reflecting an increased presence of mitochondria at sites of active migration.

These findings suggest that P188 promotes redistribution and maintenance of mitochondria in leading-edge cells, supporting localized energy availability necessary for cytoskeletal remodeling during wound closure.

Compared to controls, P188 treatment resulted in more elongated and peripheral mitochondrial networks, particularly at the leading edge of migrating cells. This redistribution likely supports localized energy production and cytoskeletal coordination required for wound closure.

3.6. P188 Promotes Cellular ATP Recovery Following CCCP-Induced Mitochondrial Damage

To determine whether the structural improvements observed in mitochondria were accompanied by functional recovery, intracellular ATP levels were measured after CCCP induced mitochondrial depolarization. Immediately following treatment, both 5 μM and 50 μM CCCP caused dose dependent ATP depletion, reducing luminescence to ~50% and ~1% of untreated control, respectively (Figure 6(a)).

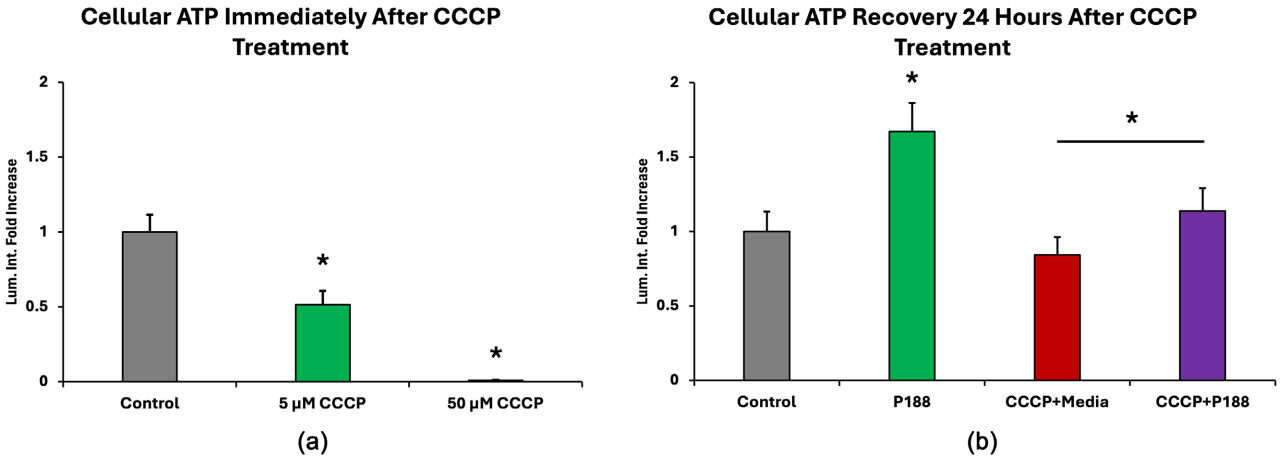

Figure 6. P188 promotes cellular ATP recovery following CCCP-induced mitochondrial damage. (a) Cellular ATP levels immediately after treatment with CCCP (carbonyl cyanide m-chlorophenyl hydrazone) at 5 μM or 50 μM for 1 hour show a dose dependent reduction in luminescence intensity relative to untreated control (*p < 0.05). (b) Cellular ATP levels measured 24 hours after 5 μM CCCP injury. P188 treatment alone significantly increased ATP levels com-pared to control (*p < 0.05). Cells treated with CCCP followed by media (CCCP + Media) or P188 (CCCP + P188) did not significantly differ from control, but ATP levels in CCCP + P188 were significantly higher than in CCCP + Media (*p < 0.05). Data are shown as fold increase of luminescence intensity (mean ± SEM, n = 3).

At 24 h post-injury, cultures maintained in media alone after CCCP damage, remained partially depleted, with ATP levels recovering to ~85% of baseline. In contrast, cells treated with 10 μM P188 demonstrated substantial restoration, reaching slightly above baseline values (Figure 6(b)). Interestingly, a 1.5-fold increase was observed with the addition of 10 μM P188 alone in undamaged cells, suggesting that treatment with the poloxamer to undamaged cells results in significantly higher levels of intracellular ATP.

Overall, treatment with P188 improved ATP recovery 24 hours after CCCP exposure, suggesting that the copolymer supports restoration of mitochondrial function. These findings indicate a possible role for P188 in maintaining energy homeostasis during cellular repair.

4. DISCUSSION

In this study, we used primary mouse brain microvascular endothelial cells (mBECs) to model endothelial injury and repair. mBECs retain key features of the in vivo brain endothelium, including tight junctions, low transcytotic activity, and polarized transport [3, 4, 12, 13] making them a relevant system for studying vascular repair. Disruption of the endothelial layer, whether by oxidative stress, trauma, or metabolic insult, can impair mitochondrial function, destabilize the cytoskeleton, and compromise barrier integrity [6, 7, 21, 22]. This breakdown facilitates pathological permeability and contributes to neurological disease progression [3, 8]. Thus, identifying strategies that enhance endothelial repair is of therapeutic interest.

To examine cellular recovery, we employed the scratch wound assay, a well-established method for assessing collective migration. This model simulates localized injury and allows visualization of wound edge dynamics, where migration, cytoskeletal reorganization, and metabolic demand are highest. Restoration of the monolayer is essential for reestablishing vascular continuity and maintaining homeostasis [9, 10].

We found that Poloxamer 188 (P188), a nonionic triblock copolymer with established membrane stabilizing properties [40], significantly enhanced wound closure in mBEC monolayers. Both 10 μM and 100 μM P188 accelerated repair, with similar efficacy, suggesting a threshold response rather than a linear dose dependency. These results align with previous studies showing P188 is effective at low micromolar concentrations, while higher doses may lead to micelle formation and membrane disruption [44].

To explore P188's intracellular effects, we used a fluorescent analog (P188-Rh110) and found that it is taken up by mBECs in an actin dependent manner. Disruption of actin filaments using Cytochalasin D markedly reduced the uptake. This is consistent with earlier findings that P188 enters cells through active transport and can localize to organelles such as lysosomes [41, 42]. Our observations further suggest that P188 preferentially accumulates in injured cells, possibly due to increased membrane permeability.

Beyond uptake, P188 treatment promoted extensive reorganization of the actin cytoskeleton. Cells treated with P188 displayed enhanced lamellipodia, more defined stress fibers, and greater protrusive activity at the wound edge, features indicative of active migration and cytoskeletal readiness for repair. These structural changes likely depend on intact mitochondrial function. Actin polymerization and myosin driven contractility are energetically costly, requiring localized ATP production that is often supplied by mitochondria positioned at sites of active remodeling. Blocking oxidative phosphorylation has been shown to decrease F-actin polymerization, impair lamellipodia formation, and slow migration [28, 45], underscoring the importance of mitochondrial ATP supply in maintaining migratory architecture.

In addition to bioenergetics, mitochondrial positioning at the leading edge is critical for efficient protrusion and adhesion turnover. Mitochondrial trafficking toward sites of actin remodeling is regulated by adaptors such as Miro-1, and depletion of Miro disrupts mitochondrial coupling to the actin cytoskeleton, impairs focal adhesion dynamics, and slows both single cell and collective migration [30]. Similarly, loss of the fission protein Drp1 alters mitochondrial distribution and Ca^{2+} homeostasis, suppressing Rho/ROCK signaling and reducing migratory efficiency [46].

Although our current data do not directly demonstrate a physical interaction between P188 and mitochondria, the strong coupling between mitochondrial function and actin remodeling raises the possibility that P188's effects extend beyond the cytoskeleton. Enhanced mitochondrial localization at the wound edge in P188 treated cells could simply reflect higher local energy demand during migration, but we cannot rule out the alternative that P188 modulates mitochondrial behavior more directly, perhaps by influencing membrane properties or signaling pathways that coordinate organelle positioning. Resolving these possibilities will require targeted experiments to determine whether mitochondrial redistribution is a consequence of actin driven metabolic demand or an independent effect of P188 on mitochondrial dynamics.

Given this correlation, we next evaluated the effects of mitochondrial depolarization with the uncoupler CCCP, allowing us to test whether P188's pro-migratory activity persists when oxidative phosphorylation and organelle positioning are compromised. Using BioTracker 488, we visualized mitochondrial morphology after injury induced by CCCP, a mitochondrial uncoupler that collapses membrane potential and inhibits oxidative phosphorylation [47]. As expected, CCCP caused pronounced mitochondrial

fragmentation and loss of organized network structure. Interestingly, cells treated with P188 following CCCP exposure displayed increased mitochondrial density and a shift toward elongated morphology at the wound edge, features consistent with enhanced trafficking and partial restoration of the network. While we cannot yet determine conclusively whether this reflects a direct action of P188 on mitochondrial membranes or an indirect effect via cytoskeletal stabilization and migration-associated demand, the localization pattern suggests improved organelle positioning in regions of active repair. Quantitatively, this was supported by higher mitochondrial fluorescence intensity in P188 treated cells compared to media controls.

To explore whether these structural changes were accompanied by functional recovery, we then measured intracellular ATP levels. As anticipated, CCCP treatment caused a dose-dependent depletion of ATP, reflecting impaired oxidative phosphorylation [48]. After 24 hours, P188 treated cells exhibited significantly greater ATP restoration than media controls, indicating that P188 facilitates not only the recovery of mitochondrial architecture but also the reestablishment of metabolic capacity following injury. Whether this improvement stems from direct support of mitochondrial integrity, enhancement of trafficking to energy demanding regions, or broader effects on cellular repair signaling remains an open question that will require targeted mechanistic studies.

5. CONCLUSIONS

Taken together, our findings support the hypothesis that Poloxamer 188 enhances endothelial wound healing not only through its well-established membrane stabilizing properties, but also by influencing intracellular processes that are critical to cellular recovery and migration. P188 treatment accelerated wound closure in mBECs, coinciding with actin-dependent cytoskeletal remodeling, lamellipodial advancement, and the redistribution of mitochondria toward the leading edge. These effects occurred in an injury context where both membrane integrity and energetic capacity are compromised, suggesting that P188's activity may extend beyond passive membrane repair to include the preservation or restoration of cellular systems that coordinate motility and energy production.

The present work cannot yet determine whether the mitochondrial responses we observed improved morphology, localization, and ATP recovery after CCCP challenge arise solely as a downstream consequence of enhanced actin mediated migration, or whether P188 also exerts more direct effects on mitochondrial membranes, trafficking machinery, or signaling pathways. Both scenarios remain plausible and carry distinct mechanistic implications.

Future studies should therefore focus on dissecting these possibilities, including assessing P188's influence on actin regulatory pathways and mitochondrial fission fusion dynamics. Given prior evidence that P188 localizes to intracellular vesicles, its potential interactions with lysosomes, endosomes, and mitochondria associated membranes warrant further investigation as possible conduits for cross organelle communication as well. Finally, translating these findings to more physiologically relevant systems, such as 3D microvascular simulations or in vivo models of blood brain barrier disruption, will be essential to fully define P188's therapeutic potential in neurovascular injury and repair.

AUTHOR CONTRIBUTIONS

Conceptualization, M. G. and M. C.; methodology, M. G. and M. C.; soft-ware, M. G. and A. A.; validation, M. G. and A. A.; formal analysis, M. G.; investigation, M. G. and M. C.; resources, M. G. and M. C.; data curation, M. G.; writing—original draft preparation, M. G.; writing—review and editing, M. G. and M. C.; visualization, M. G. and M. C.; supervision, M. C.; project administration, M. C.; funding acquisition, M. C. All authors have read and agreed to the published version of the manuscript.

FUNDING

This research was funded by generous donation from Dr. Walter Cabe and the Alfred R. and Janet H. Endowment (MC).

DATA AVAILABILITY STATEMENT

Data are available from the authors upon reasonable request.

CONFLICTS OF INTEREST

The authors declare no conflicts of interest.

REFERENCES

1. Alahmari, A. (2021) Blood-Brain Barrier Overview: Structural and Functional Correlation. *Neural Plasticity*, **2021**, Article ID: 6564585. https://doi.org/10.1155/2021/6564585
2. Andreone, B.J., Chow, B.W., Tata, A., Lacoste, B., Ben-Zvi, A., Bullock, K., *et al.* (2017) Blood-Brain Barrier Permeability Is Regulated by Lipid Transport-Dependent Suppression of Caveolae-Mediated Transcytosis. *Neuron*, **94**, 581-594.e5. https://doi.org/10.1016/j.neuron.2017.03.043
3. Zhao, Z., Nelson, A.R., Betsholtz, C. and Zlokovic, B.V. (2015) Establishment and Dysfunction of the Blood-Brain Barrier. *Cell*, **163**, 1064-1078. https://doi.org/10.1016/j.cell.2015.10.067
4. Kisler, K., Nelson, A.R., Montagne, A. and Zlokovic, B.V. (2017) Cerebral Blood Flow Regulation and Neurovascular Dysfunction in Alzheimer Disease. *Nature Reviews Neuroscience*, **18**, 419-434. https://doi.org/10.1038/nrn.2017.48
5. Johnson, V.E., Weber, M.T., Xiao, R., Cullen, D.K., Meaney, D.F., Stewart, W., *et al.* (2018) Mechanical Disruption of the Blood-Brain Barrier Following Experimental Concussion. *Acta Neuropathologica*, **135**, 711-726. https://doi.org/10.1007/s00401-018-1824-0
6. Zha, D., Wang, S., Monaghan-Nichols, P., Qian, Y., Sampath, V. and Fu, M. (2023) Mechanisms of Endothelial Cell Membrane Repair: Progress and Perspectives. *Cells*, **12**, Article 2648. https://doi.org/10.3390/cells12222648
7. Fang, Y., Hsieh, Y., Hu, C. and Tu, Y. (2023) Endothelial Dysfunction in Neurodegenerative Diseases. *International Journal of Molecular Sciences*, **24**, Article 2909. https://doi.org/10.3390/ijms24032909
8. Krueger, M., Härtig, W., Frydrychowicz, C., Mueller, W.C., Reichenbach, A., Bechmann, I., *et al.* (2016) Stroke-induced Blood-Brain Barrier Breakdown along the Vascular Tree—No Preferential Affection of Arteries in Different Animal Models and in Humans. *Journal of Cerebral Blood Flow & Metabolism*, **37**, 2539-2554. https://doi.org/10.1177/0271678x16670922
9. Qi, L., Wang, F., Sun, X., Li, H., Zhang, K. and Li, J. (2024) Recent Advances in Tissue Repair of the Blood-Brain Barrier after Stroke. *Journal of Tissue Engineering*, **15**, 1-25. https://doi.org/10.1177/20417314241226551
10. Jonkman, J.E.N., Cathcart, J.A., Xu, F., Bartolini, M.E., Amon, J.E., Stevens, K.M., *et al.* (2014) An Introduction to the Wound Healing Assay Using Live-Cell Microscopy. *Cell Adhesion & Migration*, **8**, 440-451. https://doi.org/10.4161/cam.36224
11. Michaelis, U.R. (2014) Mechanisms of Endothelial Cell Migration. *Cellular and Molecular Life Sciences*, **71**, 4131-4148. https://doi.org/10.1007/s00018-014-1678-0
12. Mentor, S., Makhathini, K.B. and Fisher, D. (2022) The Role of Cytoskeletal Proteins in the Formation of a Functional *in Vitro* Blood-Brain Barrier Model. *International Journal of Molecular Sciences*, **23**, Article 742. https://doi.org/10.3390/ijms23020742
13. Coomber, B.L. and Gotlieb, A.I. (1990) *In Vitro* Endothelial Wound Repair. Interaction of Cell Migration and Proliferation. *Arteriosclerosis: An Official Journal of the American Heart Association, Inc.*, **10**, 215-222. https://doi.org/10.1161/01.atv.10.2.215
14. Bai, Y., Zhao, F., Wu, T., Chen, F. and Pang, X. (2023) Actin Polymerization and Depolymerization in Developing

Vertebrates. *Frontiers in Physiology*, **14**, Article 1213668. https://doi.org/10.3389/fphys.2023.1213668

15. Abreu-Blanco, M.T., Watts, J.J., Verboon, J.M. and Parkhurst, S.M. (2012) Cytoskeleton Responses in Wound Repair. *Cellular and Molecular Life Sciences*, **69**, 2469-2483. https://doi.org/10.1007/s00018-012-0928-2
16. Millard, T.H. and Martin, P. (2008) Dynamic Analysis of Filopodial Interactions during the Zippering Phase of *Drosophila* Dorsal Closure. *Development*, **135**, 621-626. https://doi.org/10.1242/dev.014001
17. Le, S., Yu, M., Bershadsky, A. and Yan, J. (2020) Mechanical Regulation of Formin-Dependent Actin Polymerization. *Seminars in Cell & Developmental Biology*, **102**, 73-80. https://doi.org/10.1016/j.semcdb.2019.11.016
18. Ahangar, P., Strudwick, X.L. and Cowin, A.J. (2022) Wound Healing from an Actin Cytoskeletal Perspective. *Cold Spring Harbor Perspectives in Biology*, **14**, a041235. https://doi.org/10.1101/cshperspect.a041235
19. Rodnick-Smith, M., Luan, Q., Liu, S. and Nolen, B.J. (2016) Role and Structural Mechanism of Wasp-Triggered Conformational Changes in Branched Actin Filament Nucleation by Arp2/3 Complex. *Proceedings of the National Academy of Sciences of the United States of America*, **113**, E3834-E3843. https://doi.org/10.1073/pnas.1517798113
20. Ridley, A.J. (2015) Rho GTPase Signalling in Cell Migration. *Current Opinion in Cell Biology*, **36**, 103-112. https://doi.org/10.1016/j.ceb.2015.08.005
21. Magdalena, J., Millard, T.H., Etienne-Manneville, S., Launay, S., Warwick, H.K. and Machesky, L.M. (2003) Involvement of the Arp2/3 Complex and Scar2 in Golgi Polarity in Scratch Wound Models. *Molecular Biology of the Cell*, **14**, 670-684. https://doi.org/10.1091/mbc.e02-06-0345
22. Schaks, M., Giannone, G. and Rottner, K. (2019) Actin Dynamics in Cell Migration. *Essays in Biochemistry*, **63**, 483-495. https://doi.org/10.1042/ebc20190015
23. Zhang, B., Pan, C., Feng, C., Yan, C., Yu, Y., Chen, Z., *et al.* (2022) Role of Mitochondrial Reactive Oxygen Species in Homeostasis Regulation. *Redox Report*, **27**, 45-52. https://doi.org/10.1080/13510002.2022.2046423
24. Feissner, R.F. (2009) Crosstalk Signaling between Mitochondrial Ca^{2+} and Ros. *Frontiers in Bioscience*, **14**, 1197-1218. https://doi.org/10.2741/3303
25. Madan, S., Uttekar, B., Chowdhary, S. and Rikhy, R. (2022) Mitochondria Lead the Way: Mitochondrial Dynamics and Function in Cellular Movements in Development and Disease. *Frontiers in Cell and Developmental Biology*, **9**, Article 781933. https://doi.org/10.3389/fcell.2021.781933
26. Toyama, E.Q., Herzig, S., Courchet, J., Lewis, T.L., Losón, O.C., Hellberg, K., *et al.* (2016) AMP-Activated Protein Kinase Mediates Mitochondrial Fission in Response to Energy Stress. *Science*, **351**, 275-281. https://doi.org/10.1126/science.aab4138
27. Shannon, N., Gravelle, R. and Cunniff, B. (2022) Mitochondrial Trafficking and Redox/Phosphorylation Signaling Supporting Cell Migration Phenotypes. *Frontiers in Molecular Biosciences*, **9**, Article 925755. https://doi.org/10.3389/fmolb.2022.925755
28. Yadav, T., Gau, D. and Roy, P. (2022) Mitochondria-Actin Cytoskeleton Crosstalk in Cell Migration. *Journal of Cellular Physiology*, **237**, 2387-2403. https://doi.org/10.1002/jcp.30729
29. Cannito, S., Giardino, I., d'Apolito, M., Pettoello-Mantovani, M., Scaltrito, F., Mangieri, D., *et al.* (2025) The Multifaceted Role of Mitochondria in Angiogenesis. *International Journal of Molecular Sciences*, **26**, Article 7960. https://doi.org/10.3390/ijms26167960
30. Schuler, M., Lewandowska, A., Caprio, G.D., Skillern, W., Upadhyayula, S., Kirchhausen, T., *et al.* (2017) Miro1-mediated Mitochondrial Positioning Shapes Intracellular Energy Gradients Required for Cell Migration. *Molecular Biology of the Cell*, **28**, 2159-2169. https://doi.org/10.1091/mbc.e16-10-0741
31. Fernández Casafuz, A.B., De Rossi, M.C. and Bruno, L. (2023) Mitochondrial Cellular Organization and Shape Fluctuations Are Differentially Modulated by Cytoskeletal Networks. *Scientific Reports*, **13**, Article No. 4065.

https://doi.org/10.1038/s41598-023-31121-w

32. Gatti, P., Schiavon, C., Cicero, J., Manor, U. and Germain, M. (2025) Mitochondria- and ER-Associated Actin Are Required for Mitochondrial Fusion. *Nature Communications*, **16**, Article No. 451. https://doi.org/10.1038/s41467-024-55758-x
33. Bodratti, A. and Alexandridis, P. (2018) Formulation of Poloxamers for Drug Delivery. *Journal of Functional Biomaterials*, **9**, Article 11. https://doi.org/10.3390/jfb9010011
34. Edlich, R.F., Schmolka, I.R., Prusak, M.P. and Edgerton, M.T. (1973) The Molecular Basis for Toxicity of Surfactants in Surgical Wounds. *Journal of Surgical Research*, **14**, 277-284. https://doi.org/10.1016/0022-4804(73)90029-2
35. Rodeheaver, G.T., Kurtz, L., Kircher, B.J. and Edlich, R.F. (1980) Pluronic F-68: A Promising New Skin Wound Cleanser. *Annals of Emergency Medicine*, **9**, 572-576. https://doi.org/10.1016/s0196-0644(80)80228-9
36. Gu, J., Ge, J., Li, M., Xu, H., Wu, F. and Qin, Z. (2013) Poloxamer 188 Protects Neurons against Ischemia/Reperfusion Injury through Preserving Integrity of Cell Membranes and Blood Brain Barrier. *PLOS ONE*, **8**, e61641. https://doi.org/10.1371/journal.pone.0061641
37. Merchant, F.A., Holmes, W.H., Capelli-Schellpfeffer, M., Lee, R.C. and Toner, M. (1998) Poloxamer 188 Enhances Functional Recovery of Lethally Heat-Shocked Fibroblasts. *Journal of Surgical Research*, **74**, 131-140. https://doi.org/10.1006/jsre.1997.5252
38. Bao, H., Wang, T., Zhang, M., Liu, R., Dai, D., Wang, Y., *et al.* (2012) Poloxamer-188 Attenuates TBI-Induced Blood-Brain Barrier Damage Leading to Decreased Brain Edema and Reduced Cellular Death. *Neurochemical Research*, **37**, 2856-2867. https://doi.org/10.1007/s11064-012-0880-4
39. Bajaj, S., Shoemaker, T., Hakimiyan, A.A., Rappoport, L., Pascual-Garrido, C., Oegema, T.R., *et al.* (2010) Protective Effect of P188 in the Model of Acute Trauma to Human Ankle Cartilage: The Mechanism of Action. *Journal of Orthopaedic Trauma*, **24**, 571-576. https://doi.org/10.1097/bot.0b013e3181ec4712
40. G. Moloughney, J. and Weisleder, N. (2012) Poloxamer 188 (P188) as a Membrane Resealing Reagent in Biomedical Applications. *Recent Patents on Biotechnology*, **6**, 200-211. https://doi.org/10.2174/1872208311206030200
41. Alatrash, N., Alsup, A., Grubbs, M., Nomellini, V. and Cho, M. (2025) Active Transport of Therapeutic Triblock Amphiphilic Polymer Poloxamer 188 in Brain Endothelial Cells for Cellular Repair. *Journal of Biomedical Science and Engineering*, **18**, 301-316. https://doi.org/10.4236/jbise.2025.187022
42. Luo, C., Chen, X., Li, L., Li, Q., Li, B., Xue, A., *et al.* (2013) Poloxamer 188 Attenuates *in Vitro* Traumatic Brain Injury-Induced Mitochondrial and Lysosomal Membrane Permeabilization Damage in Cultured Primary Neurons. *Journal of Neurotrauma*, **30**, 597-607. https://doi.org/10.1089/neu.2012.2425
43. Dong, H., Qin, Y., Huang, Y., Ji, D. and Wu, F. (2019) Poloxamer 188 Rescues MPTP-Induced Lysosomal Membrane Integrity Impairment in Cellular and Mouse Models of Parkinson's Disease. *Neurochemistry International*, **126**, 178-186. https://doi.org/10.1016/j.neuint.2019.03.013
44. Inyang, E., Abhyankar, V., Chen, B. and Cho, M. (2020) Modulation of *in Vitro* Brain Endothelium by Mechanical Trauma: Structural and Functional Restoration by Poloxamer 188. *Scientific Reports*, **10**, Article No. 3054. https://doi.org/10.1038/s41598-020-59888-2
45. Zhao, J., Zhang, J., Yu, M., Xie, Y., Huang, Y., Wolff, D.W., *et al.* (2012) Mitochondrial Dynamics Regulates Migration and Invasion of Breast Cancer Cells. *Oncogene*, **32**, 4814-4824. https://doi.org/10.1038/onc.2012.494
46. Jones, E., Gaytan, N., Garcia, I., Herrera, A., Ramos, M., Agarwala, D., *et al.* (2016) A Threshold of Transmembrane Potential Is Required for Mitochondrial Dynamic Balance Mediated by DRP1 and Oma1. *Cellular and Molecular Life Sciences*, **74**, 1347-1363. https://doi.org/10.1007/s00018-016-2421-9

47. Miyazono, Y., Hirashima, S., Ishihara, N., Kusukawa, J., Nakamura, K. and Ohta, K. (2018) Uncoupled Mitochondria Quickly Shorten along Their Long Axis to Form Indented Spheroids, Instead of Rings, in a Fission-Independent Manner. *Scientific Reports*, **8**, Article No. 350. https://doi.org/10.1038/s41598-017-18582-6

48. JanssenDuijghuijsen, L.M., Grefte, S., de Boer, V.C.J., Zeper, L., van Dartel, D.A.M., van der Stelt, I., *et al.* (2017) Mitochondrial ATP Depletion Disrupts Caco-2 Monolayer Integrity and Internalizes Claudin 7. *Frontiers in Physiology*, **8**, Article 794. https://doi.org/10.3389/fphys.2017.00794